INSTITUTE OF PHYSICS PUBLISHING JOURNAL OF PHYSICS: CONDENSED MATTER

J. Phys.: Condens. Matter **14** (2002) 9339–9352 PII: S0953-8984(02)36559-7

Effective interactions and phase behaviour for a model clay suspension in an electrolyte

E Trizac[1], L Bocquet[2], R Agra[1], J-J Weis[1] and M Aubouy[3]

[1] Laboratoire de Physique Théorique, UMR CNRS 8627, Bâtiment 210, Université Paris-Sud, 91405 Orsay Cedex, France
[2] Laboratoire de Physique de l'Ens Lyon, UMR CNRS 5672, 46 Allée d'Italie, 69364 Lyon Cedex, France
[3] SI3M, DRFMC, CEA-DSM Grenoble, 17 rue des Martyrs, 38054 Grenoble Cedex 9, France

Received 2 May 2002
Published 27 September 2002
Online at stacks.iop.org/JPhysCM/14/9339

Abstract

Since the early observation of nematic phases of disc-like clay colloids by Langmuir in 1938, the phase behaviour of such systems has resisted theoretical understanding. The main reason is that there is no satisfactory generalization for charged discs of the isotropic DLVO (Derjaguin, Landau, Verwey and Overbeek) potential describing the effective interactions between a pair of spherical colloids in an electrolyte. In this paper, we show how to construct such a pair potential, incorporating approximately both the non-linear effects of counter-ion condensation (charge renormalization) and the anisotropy of the charged platelets. We discuss the consequences for the phase behaviour of laponite dispersions (thin discs of 30 nm diameter and 1 nm thickness), and we present an investigation into the mesostructure via Monte Carlo simulations.

1. Introduction

With the possibility of forming an orientational ordering, the phase behaviour of anisotropic colloids is richer than its counterpart for spherical particles. Surprisingly, the isotropic–nematic transition expected on purely entropic grounds (excluded volume effects) has been extensively reported for rod-like colloids in the last 60 years [1]. However, it could only be observed recently for discotic particles in apolar media [2]. This experimental work directly points to the subtle effect of electrostatic interactions, given that in the widely studied model system of colloidal platelets, namely aqueous clay dispersions, the isotropic/nematic phase separation is hindered by a ubiquitous 'fluid–solid' transition.

In spite of an important experimental and theoretical effort in the last ten years, triggered by the emergence of laponite as a model system for disc-like colloidal suspensions[4], the above

[4] Laponite particles may be considered as approximately monodisperse charged discs with a radius of 150 Å and a thickness of 10 Å.

0953-8984/02/409339+14$30.00

transition is far from being well understood [3–30]. In particular, the precise nature of the phases observed experimentally is debated [3, 13, 23], so that the relevance of the traditional terminology 'sol–gel' to describe the transition is somewhat controversial.

On the other hand, theoretical approaches to describe the phase behaviour of charged disc-like particles in an electrolyte are in their infancy [4, 8, 16, 21], essentially because there is no satisfactory generalization for discs of the isotropic DLVO (Derjaguin, Landau, Verwey and Overbeek) potential [31] describing the effective interactions between a pair of spherical colloids. In the simplest situation of two coaxial and parallel uniformly charged platelets, the effective Coulomb force has been computed within linear [10] and non-linear [20] Poisson–Boltzmann (PB) theory. A screened electrostatic pair potential has been worked out [32], allowing us to compute analytically the interaction energy for discs of arbitrary orientation; this approach holds at the level of linearized PB theory (weak electrostatic coupling), and is expressed as a perturbative expansion in the parameter κr_0, r_0 being the disc radius and κ the inverse Debye length in the electrolyte. It consequently becomes less reliable when κr_0 becomes of the order of one or larger (the typical situation for laponite solutions), or when the charge on the platelets becomes too large (high electrostatic coupling, also typical of clay systems). The latter limitation may be circumvented by introducing the concept of charge renormalization [31, 33–35], while the former requires the re-summation of all the powers of κr_0 involved in the 'multi-polar' expansion propounded in [32]. In this paper, we discuss how to take both aspects into account and investigate the consequences on the phase behaviour. Our goal is to understand the effect of colloid anisotropy on a possible phase transition. We show that considering electrostatic effects only and discarding van der Waals interactions yields qualitative differences between spherical and discotic colloids. We also show that the equivalent of the fluid–solid transition for spheres is nevertheless reminiscent of the 'sol–gel' transition reported in [3].

The paper is organized as follows. In section 2, we obtain a pair potential for discs valid at large distances within linearized PB theory. We show that, at asymptotically large separations, this potential remains strongly anisotropic, unlike its counterpart in vacuum or in a plain dielectric medium (no salt). The approach is generalized in section 3 to an arbitrary 'one-dimensional' or 'two-dimensional' colloid (i.e. with vanishing internal volume). The non-linear phenomenon of counter-ion 'condensation' leading to a renormalization of the bare platelet charge is then considered in section 4, and the resulting effective charge successfully tested against 'exact' numerical simulations reported in the literature. In section 5, we propose a first and simplified investigation into the phase behaviour by mapping the interaction energy on to an isotropic Yukawa potential. Finally, the full anisotropic potential, including charge renormalization, is used to investigate the mesostructure of an assembly of interacting discs by means of Monte Carlo computer simulations (section 6). Conclusions are drawn in section 7.

2. Large distance screened electrostatic potential

We consider first a unique platelet $\mathcal{P}$ of radius r_0 and surface charge σ in a 1:1 electrolyte of bulk density n (infinite dilution limit). The solvent is assumed to be a dielectric continuum of permittivity ε. Within linearized Poisson–Boltzmann (LPB) theory, the dimensionless electrostatic potential obeys the following Poisson equation

$$\nabla^2\phi = \kappa^2\phi, \tag{1}$$

where $\kappa^2 = 8\pi\ell_B n$ is the inverse Debye length squared and $\ell_B = e^2/(kT\varepsilon)$ denotes the Bjerrum length corresponding to the distance where the bare Coulomb potential felt by two

elementary point charges becomes equal to the thermal energy kT ($\ell_B \simeq 7$ Å in water at room temperature). The potential is chosen to vanish at infinity and e denotes the elementary charge.

We are interested in the behaviour of ϕ at large distances, which is relevant to describe the interactions in dilute suspensions. The solution of equation (1) has been worked out in the form of an integral representation in [10, 36], or as a multi-polar-like expansion [32]. It is however more convenient to obtain an explicit expression, which is a good starting point to derive the pair interaction. This can be achieved by writing the solution as a convolution of the surface charge of the platelets with the screened Coulomb potential:

$$\phi(\boldsymbol{r}) = \ell_B \int_{\mathcal{P}} \frac{\sigma}{e} \frac{\exp(-\kappa|\boldsymbol{r}-\boldsymbol{s}|)}{|\boldsymbol{r}-\boldsymbol{s}|}\, \mathrm{d}^2\boldsymbol{s}. \tag{2}$$

It is important to realize that such a convolution procedure would give incorrect results for polyions of non-vanishing excluded volume (e.g. spheres or rods of non-zero radii, see the appendix). Introducing the unit vector $\hat{\boldsymbol{n}}$ normal to the disc surface, and the angle $\theta \in [0, \pi/2]$ between the corresponding direction and the position vector $\boldsymbol{r}$ with the origin at the platelet centre, we obtain the leading contribution

$$\phi(\boldsymbol{r}) \overset{\kappa r \gg 1}{\sim} \ell_B Z_{bare} 2 \frac{\mathrm{I}_1(\kappa r_0 \sin\theta)}{\kappa r_0 \sin\theta} \frac{\mathrm{e}^{-\kappa r}}{r} \qquad \text{with } Z_{bare} e = \pi r_0^2 \sigma, \tag{3}$$

where I_1 denotes the modified Bessel function of the first kind, such that $\mathrm{I}_1(x) \sim x/2$ for $|x| \ll 1$. A peculiarity of the screened Coulomb potential appears at this point: whereas the large r potential becomes isotropic and behaves as Z_{bare}/r in vacuum (a situation corresponding to the limit $\kappa \to 0$), the anisotropy is present at all distances in an electrolyte ($\kappa \neq 0$); the θ and r dependences factorize in equation (3). In practice, the anisotropy of the potential is generically significant when the size of the object under consideration is larger than the Debye length (i.e. $\kappa r_0 > 1$ here). For laponite discs of radius 150 Å this crossover corresponds to an ionic strength $I^* = 10^{-4}$ M. As noted in [17], I^* corresponds experimentally to a threshold value delimiting qualitatively different phase behaviours. At fixed distance r, the potential (3) is minimum for $\theta = 0$ which corresponds to the configuration where the 'average' distance between the point where ϕ is computed and the platelet is maximal. On the other hand, the potential is maximum for $\theta = \pi/2$. From equation (3) the ratio between these extremal values is r-independent, and reads $2\mathrm{I}_1(\kappa r_0)/(\kappa r_0)$ which can be as large as 10 for $\kappa r_0 = 5$ (important anisotropy).

This result may be used to compute the potential energy of interactions between two platelets A and B with arbitrary relative orientations, as shown in figure 1. This energy is obtained by integrating the screened potential created by disc A defined by equation (3) over the surface charge distribution of the second disc (B)

$$V_{AB}(r, \theta_A, \theta_B) = \int_B \frac{\sigma}{e} \phi_A(\boldsymbol{r}+\boldsymbol{s})\, \mathrm{d}^2\boldsymbol{s}, \tag{4}$$

where V_{AB} is the dimensionless potential expressed in kT units. Again, such a procedure would not give the proper interactions in the case of polyions with internal volume. At large distances, we obtain

$$V_{AB}(r, \theta_A, \theta_B) \sim Z_{bare}^2 \ell_B 4 \frac{\mathrm{I}_1(\kappa r_0 \sin\theta_A)}{\kappa r_0 \sin\theta_A} \frac{\mathrm{I}_1(\kappa r_0 \sin\theta_B)}{\kappa r_0 \sin\theta_B} \frac{\mathrm{e}^{-\kappa r}}{r}. \tag{5}$$

Clearly, the relative orientation of the platelets is not completely specified by the three parameters r, θ_A and θ_B, but the omitted Euler angles only appear in higher-order terms, such as $\exp(-\kappa r)/r^2$, $\exp(-\kappa r)/r^3 \ldots$. In particular, the energy (5) appears insensitive to a precession of the discs around their centre-to-centre direction.

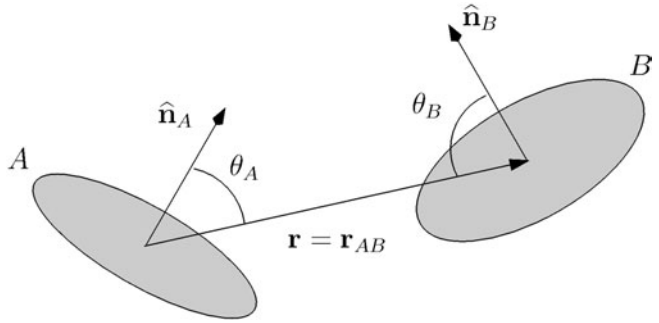

Figure 1. Definition of the coordinates used in the two-body problem.

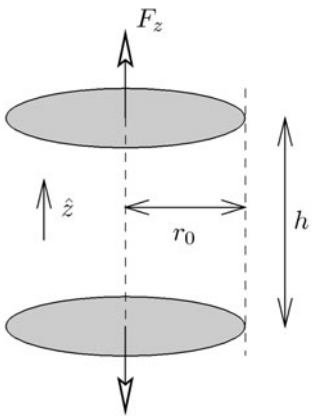

Figure 2. Geometry used to compute the force between two discs in section 4.

At fixed centre-to-centre distance, the above energy (always repulsive [37]) is maximized for co-planar discs ($\theta_A = \theta_B = \pi/2$, which corresponds to the maximum overlap of electric double layers) and minimized when the discs are co-axial and parallel ($\theta_A = \theta_B = 0$, see the configuration represented in figure 2). A situation of intermediate electrostatic energy is that of T-shape perpendicular discs ($\theta_A = 0$ and $\theta_B = \pi/2$). These results are consistent with the numerical LPB pair potential reported in [36], where it was also shown that the interactions between platelets at constant surface charge or constant potential were qualitatively very similar.

In [32], the potential energy V_{AB} was obtained in the form of a multi-polar expansion. Unlike its unscreened counterpart where the multipole of order l has a $1/r^{l+1}$ large distance contribution to the potential, this expansion is such that the multipole of order l contributes to orders $\exp(-\kappa r)/r$, $\exp(-\kappa r)/r^2 \ldots \exp(-\kappa r)/r^{l+1}$. The large r potential can, in principle, be obtained by re-summation of all multi-polar contributions, which should lead to expression (5). Alternatively, truncating the multi-polar expansion at a given order amounts to expanding (5) in powers of κr_0. Including monopole–monopole, monopole–quadrupole and quadrupole–quadrupole interactions, the following expression was obtained in [32]:

$$V_{AB}(r, \theta_A, \theta_B) = Z_{bare}^2 \ell_B \left[1 + \frac{\kappa^2 r_0^2}{8}(\sin^2\theta_A + \sin^2\theta_B) + \frac{\kappa^4 r_0^4}{64}(\sin^2\theta_A \sin^2\theta_B) \right] \frac{\mathrm{e}^{-\kappa r}}{r}. \qquad (6)$$

From equation (5), we obtain

$$V_{AB}(r,\theta_A,\theta_B) = Z_{bare}^2 \ell_B \left[1 + \frac{\kappa^2 r_0^2}{8}(\sin^2\theta_A + \sin^2\theta_B) + \frac{\kappa^4 r_0^4}{64}\left(\sin^2\theta_A \sin^2\theta_B + \frac{1}{3}\sin^4\theta_A \sin^4\theta_B \right) + \mathcal{O}(\kappa^6 r_0^6) \right] \frac{\mathrm{e}^{-\kappa r}}{r}. \tag{7}$$

Both expressions agree at order $(\kappa r_0)^2$, and the difference at order $(\kappa r_0)^4$ is the monopole–hexadecapole contribution which has not been included in equation (6). This comparison illustrates the perturbative nature of the potential derived in [32], and the fact that the corresponding multi-polar contributions are implicitly re-summed in expression (5).

3. Generalization to a polyion of arbitrary shape

The method used in the previous section may be generalized to find the far-field electrostatic potential of an arbitrary polyion with vanishing internal volume and bare charge $Z = \int_{polyion} \sigma(\boldsymbol{s})\, \mathrm{d}^2\boldsymbol{s}$. In general, the convolution solution (2) admits the large distance behaviour:

$$\phi(\boldsymbol{r}) \sim Z\ell_B f(\hat{\boldsymbol{r}},\kappa)\frac{\mathrm{e}^{-\kappa r}}{r} + \mathcal{O}\left(\frac{\mathrm{e}^{-\kappa r}}{r^2}\right) \qquad \text{for } \kappa r \gg 1. \tag{8}$$

In this expression, the anisotropic part of the potential again factorizes from the r-dependence and is given by

$$f(\hat{\boldsymbol{r}},\kappa) = \int_{polyion} \frac{\sigma(\boldsymbol{s})}{Ze} \exp(-\kappa\hat{\boldsymbol{r}}\cdot\boldsymbol{s})\, \mathrm{d}^2\boldsymbol{s}, \tag{9}$$

where $\hat{\boldsymbol{r}}$ denotes a unit vector in the direction of the position $\boldsymbol{r}$ where the potential is computed, and $\sigma(\boldsymbol{s})$ is the surface charge density at point $\boldsymbol{s}$ on the colloid. As expected, the isotropic bare Coulomb potential is recovered in the limit of low electrolyte density

$$\lim_{\kappa\to 0} f(\hat{\boldsymbol{r}},\kappa) = 1, \tag{10}$$

where Z is the bare charge.

For a circle of radius r_0 and uniform line charge, we find

$$f(\theta,\kappa r_0) = \mathrm{I}_0(\kappa r_0 \sin\theta), \tag{11}$$

where θ is the angle between $\boldsymbol{r}$ and the normal to the plane containing the circle. Finally, for a uniformly charged rod of vanishing radius and length $2l$

$$f(\theta,\kappa l) = \frac{\sinh(\kappa l\cos\theta)}{\kappa l\cos\theta}, \tag{12}$$

where θ is now the angle between $\boldsymbol{r}$ and the rod direction.

4. Towards charge renormalization for platelets

The bare charge of laponite platelets can be considered to be of the order of $Z_{bare} = 700$–1000 negative elementary charges [22, 23]. At the level of the PB approximation, this corresponds to a high electrostatic coupling (ϕ larger than unity [12, 20]), where the linearization procedure underlying equation (1) fails. However, a few Debye lengths away from the colloid, the potential has sufficiently decreased so that equation (1) is recovered and the one-body potential takes the form

$$\phi(r,\theta) = Z_{eff} f(\theta,\kappa r_0)\frac{\mathrm{e}^{-\kappa r}}{r}.$$

The effective charge Z_{eff} is (in absolute value) smaller than the bare one [33–35]. Within PB theory, it saturates to a value independent of Z_{bare} if the latter quantity is large enough. The contribution embodied in $f(\theta, \kappa r_0)$ results from the anisotropy of the colloid, and is *a priori* an unknown function. In the limit of small electrostatic coupling (small Z_{bare}) where $Z_{eff}/Z_{bare} \to 1$ by definition, the results of section 2 show that $f(\theta, X) = 2\mathrm{I}_1(X \sin\theta)/(X \sin\theta)$. On the other hand, at higher Z_{bare} corresponding to the saturation regime, the functional form of $f(\theta, X)$ is the signature of the effective charge distribution on the platelet and is related to possible differences in counter-ion condensation around the centre of the discs or in the vicinity of the edges.

It has been shown within PB theory that, in the colloidal limit $\kappa r_0 > 1$, highly charged colloids behave, as far as their far field is concerned, as constant potential particles whose value is close to $4kT/e$ (i.e. $\phi = 4$), irrespective of shape (planar, cylindrical, spherical) [38]. This prescription may be applied to the present case, with the restriction that, to our knowledge, the LPB problem cannot be solved analytically with the boundary condition of constant surface potential. However, the potential associated with the constant surface charge boundary condition provides a reasonable first approximation providing the correct qualitative variation of the effective charge with physico–chemical parameters. The corresponding anisotropic contribution to the large distance field is that computed in section 2 and the calculation of Z_{eff} follows from the knowledge of $\phi(r = 0)$. From the analytical expression reported in [10], we obtain the saturation value of Z_{eff}

$$Z_{eff}^{saturation} = Z_{sat} = \frac{r_0}{\ell_B} \frac{2\kappa r_0}{1 - \exp(-\kappa r_0)}. \tag{13}$$

It is worth noting that for a typical salt concentration corresponding to $\kappa r_0 = 1$, $Z_{sat} \simeq 100$, which is an order of magnitude smaller than the bare charge. This asymmetry guarantees that the effective charge is in the saturation regime where it no longer depends on the value of Z_{bare} [33, 38] (the precise experimental determination of Z_{bare} is therefore not required). This saturation picture is expected to be reliable in a 1:1 electrolyte (the PB mean-field approximation generally fails in electrolytes of higher valence), when there is a clear scale separation between the Bjerrum length and the size of the charged object (this constraint being fulfilled for laponite) [39].

The above prediction may be checked by inserting Z_{sat} into the analytical expression giving the LPB force between two parallel platelets [10] (configuration depicted in figure 2)

$$\frac{r_0 F_z}{kT} = \frac{4\pi \ell_B}{r_0} Z_{sat}^2 \int_0^\infty J_1^2(x) \frac{1}{x} \exp\left\{ -(h/r_0)\sqrt{x^2 + \kappa^2 r_0^2} \right\} \mathrm{d}x \tag{14}$$

and by comparing the results with the Monte Carlo simulations of Meyer *et al* [22], who considered the situation of vanishing salt. In this limit, where the quality of our prescription for Z_{eff} is expected to deteriorate, we obtain from equation (13) $Z_{sat} \to 2r_0/\ell_B \simeq 42$. The comparison is displayed in figure 3 which shows good agreement. Neglect of charge renormalization effects leads to an overestimation of the force by more than two orders of magnitude (more precisely, by a factor of $(Z_{bare}/Z_{sat})^2$—see the difference between the dashed and dotted curves in figure 3), which points to the prime importance of such a phenomenon.

5. Tentative investigation into the phase behaviour

At this point, it is interesting to investigate at least qualitatively the difference in the phase behaviour between spherical and disc-like charge stabilized colloids. For spheres, the fluid–solid transition driven by repulsive electrostatic interactions favours the isotropic fluid upon

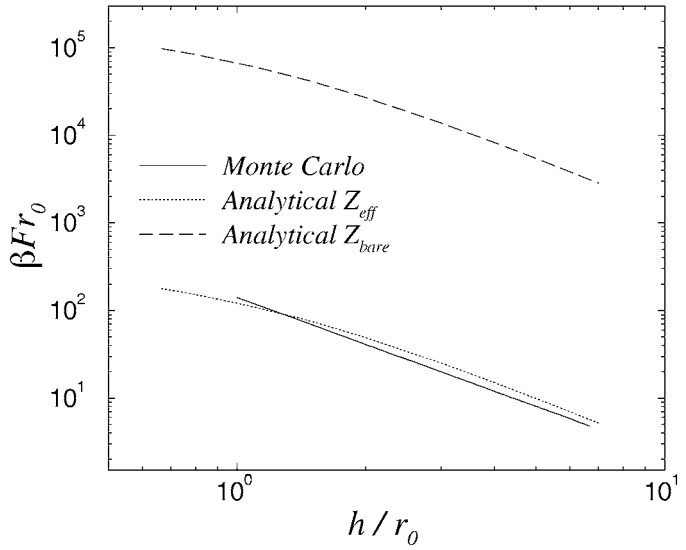

Figure 3. Comparison of the effective force between two parallel and coaxial platelets obtained by (N, V, T) Monte Carlo simulations in [22], with the general expression for the LPB force supplemented with the effective charge given by equation (13). h is the distance between the two plates (see figure 2). The same results are shown neglecting charge renormalization, which amounts to considering $Z_{eff} = Z_{bare}$ (upper dashed curve).

addition of salt in the solution [40]. The opposite is observed for laponite dispersions, where an increase of the ionic strength lowers the density where the 'solid' phase appears [3, 11]. Given that van der Waals interactions are believed to be irrelevant in the corresponding parameter range [11], this effect (illustrated in figure 4) appears at first to contradict standard DLVO phenomenology, where a screening of electrostatic repulsion (decrease of Debye length κ^{-1}) is expected to promote the simple fluid phase (sol), as occurs for spheres. However, the effective charge of an arbitrary charged object is generically a growing function of salt concentration (see, for instance, expression (13), which increases with κ), as a result of an enhanced screening of colloid/micro-ion attraction which diminishes the amount of counter-ion 'condensation'. This increase of the effective charge favours the solid phase and is thus antagonistic to the above-mentioned decrease of the range of electrostatic repulsion driven by the decrease of κ^{-1}. The competition between the increase of the amplitude of repulsion and the decrease of its range upon adding salt is a possible scenario to interpret the phase behaviour of discs, within the DLVO picture and without any attractive interactions. More quantitative results are given below.

In the following analysis, we treat spheres and discs on an equal footing (both are considered to have the same radius r_0). From the above analysis, we consider the following pair potential for discs

$$V_{AB}(r, \theta_A, \theta_B) = Z_{sat}^2 \ell_B 4 \frac{\mathrm{I}_1(\kappa r_0 \sin\theta_A)}{\kappa r_0 \sin\theta_A} \frac{\mathrm{I}_1(\kappa r_0 \sin\theta_B)}{\kappa r_0 \sin\theta_B} \frac{\mathrm{e}^{-\kappa r}}{r}, \tag{15}$$

where Z_{sat} is given by equation (13). Its counterpart for charged spheres is the standard isotropic DLVO expression [31, 35]

$$V_{AB}(r) = Z_{sat}^2 \ell_B \left(\frac{\mathrm{e}^{\kappa r_0}}{1 + \kappa r_0} \right)^2 \frac{\mathrm{e}^{-\kappa r}}{r}, \tag{16}$$

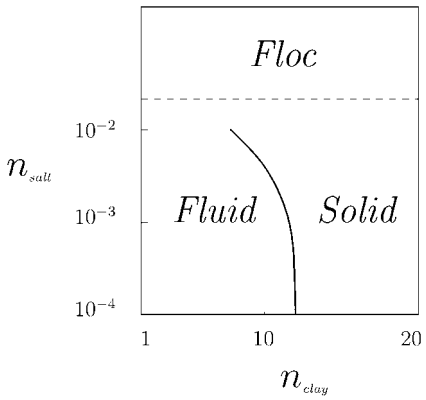

Figure 4. Schematic phase diagram of laponite suspensions, reproduced from [3], where the fluid–solid transition was referred to as a sol–gel transition. The salt concentration on the y-axis is expressed in mol $(\mathrm{dm})^{-3}$, and the scale for laponite concentrations on the x-axis is in g l^{-1}. The solid under consideration is isotropic but, at higher clay densities, a nematic solid may be formed [6]. The corresponding diagram for spherical colloids would exhibit a fluid/solid line of opposite (positive) slope [40].

where the saturation value of the effective charge has been derived analytically in [38] as a function of salt concentration (we again consider colloids with a high bare charge such that Z_{eff} coincides with its saturation value).

Given that the phase behaviour of particles interacting through Yukawa-like potentials has been extensively explored by computer simulations [41–43], we can readily obtain the melting density corresponding to a given salt concentration for the potential (16). The results (corresponding to spherical colloids) are shown in figure 5. A related procedure may be used to estimate qualitatively the position of the melting or freezing line for discs by assuming that, at low clay density (typically where the fluid/solid transition takes place for laponite suspensions), the rotational motion of the platelets occurs on a shorter timescale than the translational motion. Thus, these objects feel an effective potential resulting from the angular average of the expression given in equation (15), namely

$$V_{AB}^{average}(r) = \langle V_{AB}(r,\theta_A,\theta_B)\rangle_{\theta_A,\theta_B} = \tfrac{1}{4}\int_0^\pi \sin\theta_A \,\mathrm{d}\theta_A \int_0^\pi \sin\theta_B \,\mathrm{d}\theta_B \, V_{AB}(r,\theta_A,\theta_B)$$
$$= Z_{sat}^2 \ell_B 4\left(\frac{\cosh(\kappa r_0)-1}{\kappa^2 r_0^2}\right)^2 \frac{\mathrm{e}^{-\kappa r}}{r}. \qquad (17)$$

In doing so, we obtain an isotropic Yukawa potential where the energy scale—the term in parentheses in equation (17)—reflects the original anisotropy of the pair potential. In the standard DLVO potential (16) for spheres, the energy scale (the term $\exp(\kappa r_0)/(1+\kappa r_0)$) also depends on Debye length, but has a different physical origin and results from the exclusion of micro-ions from the interior of the spheres. Making use of the numerical Yukawa phase diagram [41–43], we obtain the melting line represented in figure 5 for the averaged potential (17), where the threshold density decreases when the salt concentration (or equivalently κ) increases, at least for $\kappa d < 4$. At the same level of description, spherical colloids show the opposite behaviour, for all values of κd. (We also emphasize that, for the spherical colloids used in the experiments of Monovoukas and Gast [40], the equivalent of the melting line reported in figure 5 is in excellent agreement with its experimental counterpart [38].)

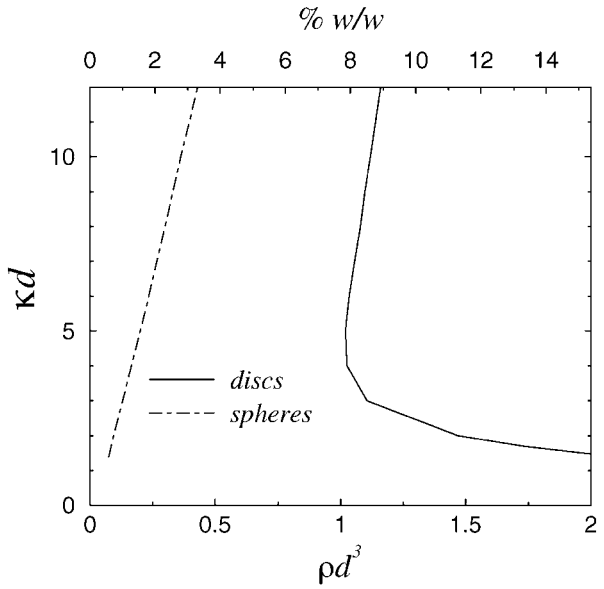

Figure 5. Tentative phase diagram of highly charged colloids in a 1:1 electrolyte, as obtained for particles interacting through a Yukawa potential in [41–43]. The equivalent of the fluid–solid transition for spheres is shown for discs (i.e. the underlying Yukawa potential is given by equation (16) for spheres and by equation (17) for discs). Discs and spheres have the same radius $r_0 = 150$ Å (reasonable for laponite clays), and $d = 2r_0$ denotes the diameter. The bottom x-label corresponds to the dimensionless number density, while the upper x-scale converts this quantity in terms of the ratio of clay mass over solvent mass for laponite platelets (this scale is consequently irrelevant for spherical colloids). In both cases, the line shown is the melting curve delimiting a solid at high density and a fluid for more dilute suspensions.

For both spheres and discs, the pre-factor of the Yukawa term $\exp(-\kappa r)/r$ is an increasing function of κ (see equations (16) and (17)). The subtle interplay between this increase and the decrease of Debye length is nevertheless able to produce a 're-entrant' melting line for discs only. In the limit of low κr_0, both expressions (16) and (17) become $\ell_B Z_{sat}^2 \exp(-\kappa r)/r$; the melting lines for spheres and discs however do not merge in this limit in figure 5, due to the difference in the limiting values of Z_{sat} for both geometries.

This approach, which consists of averaging the two-body platelet potential over angular degrees of freedom, predicts a qualitative change in the phase behaviour of platelet systems for a reduced density $\rho^* = \rho d^3$ of the order of one, which corresponds to a clay mass fraction of 8% for laponite with diameter $d = 300$ Å; see the upper x-label of figure 5. This density is approximately four times higher than the maximum density delimiting the fluid and solid regions in the phase diagram of laponite suspensions (see figure 4 and [3, 11]). So the present approach does not allow a quantitative comparison with experiments. It is however worth noting that a density $\rho^* \simeq 1$ is much smaller than the isotropic/nematic coexistence density for uncharged plates ($\rho^* \simeq 4$, [44, 45]). At this stage, it is impossible to be more specific concerning the nature of the 'solid' phase supplementing the fluid phase at high densities. This question is addressed in the following section using computer simulations.

6. Mesostructure: Monte Carlo simulations

We have implemented standard Monte Carlo simulations with typically $N = 500$ platelets interacting through the potential (15) where Z_{sat} is given by equation (13). This allows us to

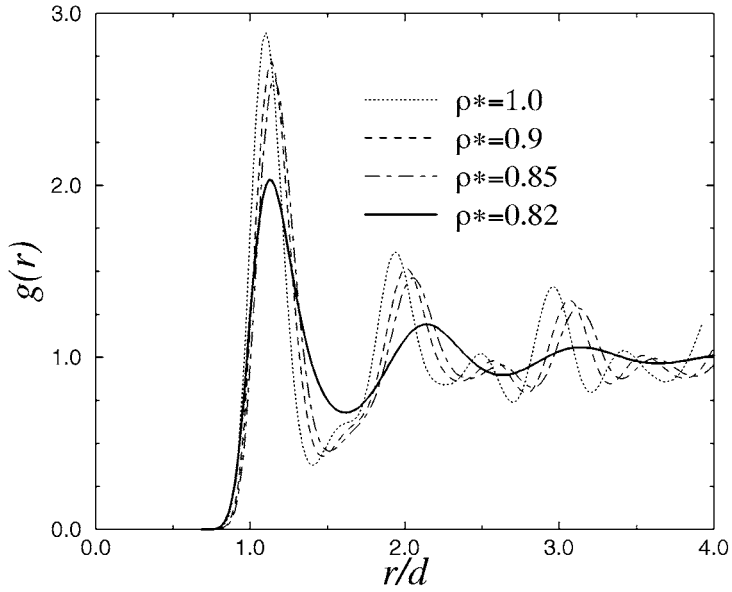

Figure 6. Centre-to-centre pair correlation function as a function of distance for $\kappa d = 1$.

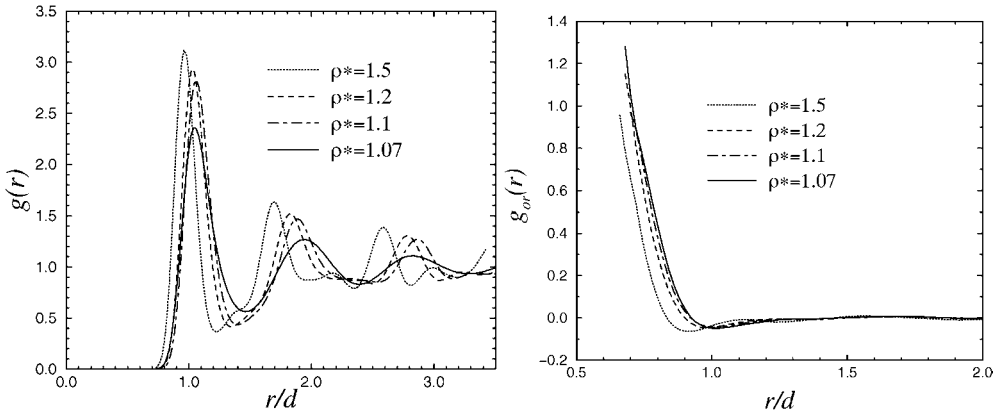

Figure 7. Same as figure 6 for a higher salt concentration ($\kappa d = 3$). The structureless orientational distribution is shown for completeness in the graph on the right.

test the validity of the approach proposed in section 5, where the initial anisotropic potential was mapped on to the isotropic Yukawa function (17). A typical run consisted of 10^5 cycles (both random displacement and rotation of the N particles).

For different values of salt concentration and platelet density, two diagnostics were used to characterize the simulated samples. Firstly, the centre-to-centre pair distribution function $g(r)$ was computed. Secondly, the orientational ordering was quantified through the statistical average of (twice) the second Legendre polynomial $P(\psi) = 3\cos^2\psi - 1$ at a given centre-to-centre distance r, where ψ is the angle formed by the normals to the two discs. The orientational pair correlation function denoted $g_{or}(r)$ follows from averaging over all pairs of platelets.

The corresponding information on the mesostructure is displayed in figures 6 and 7 for different densities and two values of κ. A striking observation is that a slight increase of the

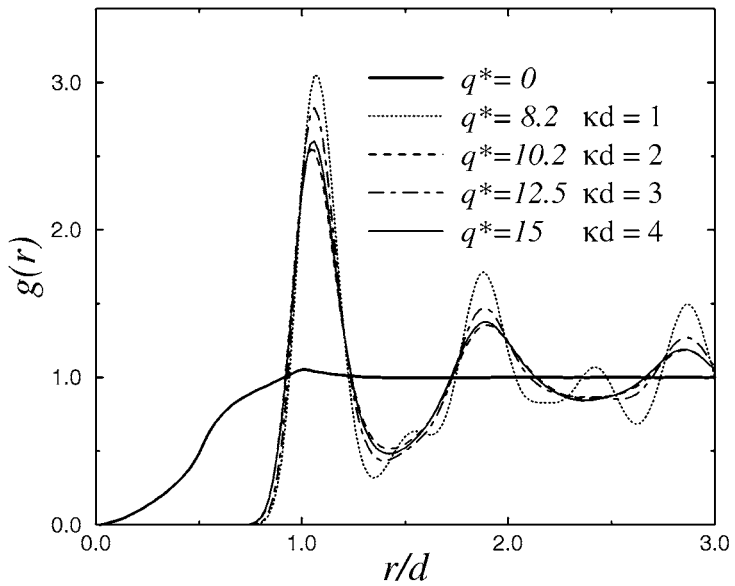

Figure 8. Pair distribution function for $\rho^* = 1.1$. The reduced charges defined as $q^* = Z_{sat}\sqrt{\ell_B/d}$ have been computed from equation (13) and are given for completeness for every κ. Also shown is $g(r)$ for an uncharged platelet system at the same density (only excluded volume effects).

density induces an important increase of the structure (see the differences between the curves at $\rho^* = 0.82$ and 0.85 in figure 6; the same is seen at $\kappa d = 3$ in figure 7 when the reduced density changes from 1.07 to 1.10). Such values of ρ^* lie close to the threshold $\rho^* = 1$ estimated in section 5. The associated orientational distributions (not shown) are structureless for the densities considered here. These results indicate a qualitative change in the structure of the fluid phase upon increasing the density, but it is still difficult to characterize the new 'phase' emerging without a thermodynamical study.

We have tested the relevance of the scenario propounded at the beginning of section 5 (competition between an increase of the amplitude and a decrease of the range of the pair potential when κ—or equivalently n_{salt}—increases). For a given density ($\rho^* = 1.1$), the pair correlation functions are monitored for various values of κ. The corresponding charges change with κ, according to equation (13). Figure 8 shows an interesting feature. As expected, the structure is most pronounced for the lowest κ, and decreases when κ increases (see the difference between the curves for $\kappa d = 1$ and 2). However, when salt concentration is further raised to $\kappa d = 3$, the maximum of $g(r)$ and the whole structure are enhanced, before decreasing again when $\kappa d = 4$. The effect evidenced in figure 8 is reminiscent of the 'anomalous' slope of the phase diagram reproduced in figure 4, and is in qualitative agreement with the simplified phase diagram drawn in figure 5.

Finally, we have performed exploratory runs at higher densities where a nematic phase would be observed in the uncharged system. The results of figure 9 for a high density $\rho^* = 5.0$ show a rich local structure both for the $g(r)$ and the orientational $g_{or}(r)$, very different from that observed at lower densities. The reference uncharged system ($q^* = 0$) with its strong nematic plateau is displayed for comparison. The inclusion of electrostatic interactions preserves the long-range nematic order, but decreases its strength (the height of the plateau). Such a nematic order was clearly absent at lower densities (see figure 7). The peaks of $g(r)$ appear correlated to those of $g_{or}(r)$, which points to the existence of oriented micro-domains with parallel platelets, and a higher nematic order than the mean one. The complex behaviour of

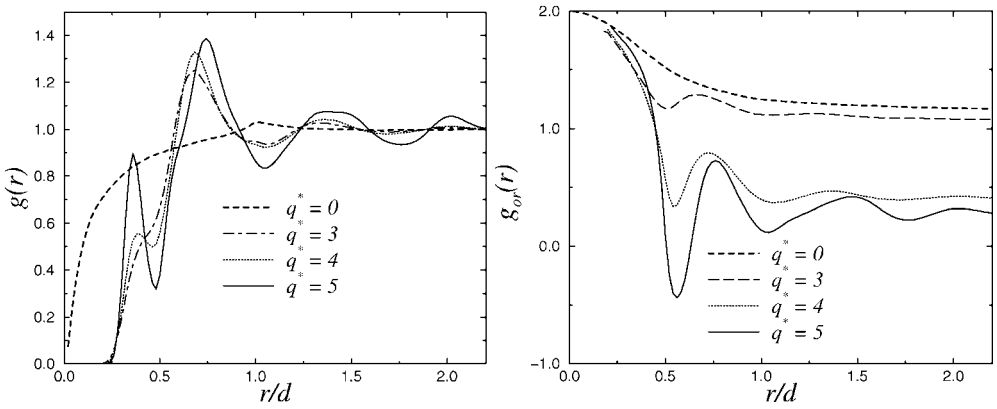

Figure 9. Effect of charge on the distributions $g(r)$ and $g_{or}(r)$, for $\rho^* = 5.0$ and a fixed screening length $\kappa d = 8$.

the distribution functions of figure 9 calls for more thorough investigations at high densities. In particular, the validity of the large distance expansion (15) may be questionable at high ρ^*.

7. Conclusion

In this paper, we have devised an electrostatic pair potential for both highly anisotropic and highly charged objects (of vanishing internal volume) based on LPB theory. For the example of infinitely thin platelets, we show that the anisotropic shape of the object results in an anisotropic Yukawa potential even at large distances. The anisotropy is an increasing function of κr_0 and becomes very marked in the colloidal limit $\kappa r_0 > 1$. To account for the non-linearities in the PB theory, when the bare charge of the platelets is large, we introduce an effective or renormalized charge. This approximation yields an effective pair potential for highly charged platelets.

The addition of salt generically results in two antagonistic effects, irrespective of colloid geometry: the range of the effective potential decreases, but its amplitude increases. This interplay appears to be quite subtle, and is able to discriminate between spherical and disc-like colloids by producing a re-entrant melting line for discs. This phenomenon appears at first incompatible with the naive DLVO expectation. Moreover, the corresponding threshold density for discs is smaller than the isotropic/nematic coexistence for uncharged plates, but still higher than its experimental 'fluid/solid' counterpart.

Preliminary results of Monte Carlo simulations for particles interacting through an anisotropic potential provide information on the mesoscopic structure of the dense phase. In particular, we show that the resulting structure is very sensitive upon increasing the density. We have also observed a 're-entrant' melting curve. These effects are in qualitative agreement with the experimental phase diagram of laponite suspensions found in the literature, even if this topic is still under debate.

Our approach suffers from several weaknesses:

(a) the non-linearities in the PB theory are accounted for at the level of charge renormalization;
(b) in this framework, we expect the effective charge to be better approximated with an anzatz where the particle effectively behaves as a constant electrostatic potential object [38], whereas we considered the platelets to be of constant surface charge;
(c) we work at the level of pair potential, and correlation effects beyond the mean-field PB approach might play a role;

(d) the precise role of van der Waals forces has not been assessed, and remains obscure for clay platelets.

Further theoretical and numerical work is needed, but we hope that the arguments presented here provide a first hint at the full problem. At least, our results strongly suggest that the combined effect of anisotropy and charge condensation have a significant and non-trivial qualitative influence on the phase diagram of highly charged colloids. These features could well be of prime importance in our understanding of the thermodynamics of clay suspensions.

Acknowledgments

We thank J-P Hansen, H Lekkerkerker, P Levitz, A Delville, D Bonn, T Nicolai, B Jancovici and F van Wijland for fruitful discussions.

Appendix

In this appendix, we show that the solution of equation (1) is not given by convolution product (2) for polyions having a non-zero internal volume. For simplicity, we consider a charged hard sphere of radius r_0 (which consequently excludes micro-ions from its interior), with a uniform surface charge σ. The solution of equation (1) takes the well-known DLVO form

$$\phi(r) = Z\ell_B \frac{\mathrm{e}^{\kappa r_0}}{1+\kappa r_0}\frac{\mathrm{e}^{-\kappa r}}{r}, \tag{A.1}$$

where $Ze = 4\pi r_0^2\sigma$ denotes the total bare charge. Alternatively, the convolution route of equation (2) yields

$$\phi_{convol}(r) = \ell_B \int_{\mathcal{P}} \frac{\sigma}{e}\frac{\exp(-\kappa|\boldsymbol{r}-\boldsymbol{s}|)}{|\boldsymbol{r}-\boldsymbol{s}|}\,\mathrm{d}^2\boldsymbol{s} \tag{A.2}$$

$$= Z\ell_B \frac{\sinh(\kappa r_0)}{\kappa r_0}\frac{\mathrm{e}^{-\kappa r}}{r} \qquad \text{for } r \geqslant r_0. \tag{A.3}$$

The origin of this discrepancy comes from the fact that upon summing up the elementary surface contributions in equation (A.2), the micro-ions are allowed to enter the 'interior' region $r \leqslant r_0$. The field created is thus that of the shell with charge Z (the colloid) plus that of the 'plasma' inside. The corresponding interior charge Z_{in} is easily computed from the expression of the electrostatic potential for $r \leqslant r_0$, which follows from a simple permutation of r and r_0 in expression (A.3)

$$\phi^{inside}_{convol}(r) = Z\ell_B \frac{\sinh(\kappa r)}{\kappa r}\frac{\mathrm{e}^{-\kappa r_0}}{r_0}. \tag{A.4}$$

We obtain

$$Z_{in} = -\frac{\kappa^2}{4\pi\ell_B}\int_0^{r_0} \phi^{inside}_{convol}(r)\,\mathrm{d}^3\boldsymbol{r} \tag{A.5}$$

$$= -Z\mathrm{e}^{-\kappa r_0}\left[\cosh(\kappa r_0) - \frac{\sinh(\kappa r_0)}{\kappa r_0}\right]. \tag{A.6}$$

Gathering results, a straightforward calculation allows us to rewrite equation (A.3) in the form

$$\phi_{convol}(r) = Z\ell_B \frac{\sinh(\kappa r_0)}{\kappa r_0}\frac{\mathrm{e}^{-\kappa r}}{r} = (Z+Z_{in})\ell_B \frac{\mathrm{e}^{\kappa r_0}}{1+\kappa r_0}\frac{\mathrm{e}^{-\kappa r}}{r}, \tag{A.7}$$

so that the DLVO structure of expression (A.1) is recovered.

The argument given here bears some similarities with the proof of the equivalence between two charged hard spheres models with a uniform background [46] (note that the equivalent of the background, the micro-ion density, is not uniform in the present situation). Finally, a related remark is that application of expression (4) for spheres does not give the DLVO pair potential (16) even if the correct one body potential (A.1) is used (use of expression (A.2) is equally incorrect). A simple way to recover (16) is through the stress tensor [31].

References

[1] Bernal J D and Fankuchen I 1941 *J. Gen. Physiol.* **25** 111
[2] Van der Kooij F M and Lekkerkerker H N W 1998 *J. Phys. Chem.* B **102** 7829
[3] Mourchid A, Delville A, Lambard J, Lécolier E and Levitz P 1995 *Langmuir* **11** 1942
[4] Dijkstra M, Hansen J-P and Madden P 1995 *Phys. Rev. Lett.* **75** 2236
[5] Trizac E and Hansen J-P 1996 *J. Phys.: Condens. Matter* **8** 9191
[6] Gabriel J-C, Sanchez C and Davidson P 1996 *J. Phys. Chem.* **100** 11 139
[7] Pignon F, Piau J M and Magnin A 1996 *Phys. Rev. Lett.* **56** 3281
[8] Dijkstra M, Hansen J-P and Madden P 1997 *Phys. Rev.* E **55** 3044
[9] Hansen J P and Trizac E 1997 *Physica* A **235** 257
[10] Trizac E and Hansen J-P 1997 *Phys. Rev.* E **56** 3137
[11] Mourchid A, Lécolier E, van Damme H and Levitz P 1998 *Langmuir* **14** 4718
[12] Leote de Carvalho R J F, Trizac E and Hansen J-P 1998 *Europhys. Lett.* **43** 369
[13] Bonn D, Kellay H, Tanaka H, Wegdam G and Meunier J 1999 *Langmuir* **15** 7534
[14] Fossum J O 1999 *Physica* A **270** 270
[15] Saunders J M, Goodwin J W, Richardson R M and Vincent B 1999 *J. Phys. Chem.* B **103** 9211
[16] Kutter S, Hansen J-P, Sprik M and Boek E 2000 *J. Chem. Phys.* **112** 311
[17] Levitz P, Lécolier E, Mourchid A, Delville A and Lyonnard S 2000 *Europhys. Lett.* **49** 672
[18] Nicolai T and Coccard S 2000 *Langmuir* **16** 8189
[19] Knaebel A, Bellour M, Munch J-P, Viasnoff V, Lequeux F and Harden J L 2000 *Europhys. Lett.* **52** 73
[20] Leote de Carvalho R J F, Trizac E and Hansen J-P 2000 *Phys. Rev.* E **61** 1634
[21] Harnau L, Costa D and Hansen J-P 2001 *Europhys. Lett.* **53** 729
[22] Meyer S, Levitz P and Delville A 2001 *J. Phys. Chem.* B **105** 10 684
[23] Nicolai T and Coccard S 2001 *Eur. Phys. J.* E **5** 221
[24] Nicolai T and Coccard S 2001 *J. Colloid Interface Sci.* **244** 51
[25] Bellon L, Ciliberto S and Laroche C 2001 *Europhys. Lett.* **53** 511
[26] Abou B, Bonn D and Meunier J 2001 *Phys. Rev.* E **64** 021510
[27] Léger D and Levesque D 2002 *J. Chem. Phys.* **116** 2251
[28] Cousin F, Cabuil V and Levitz P 2002 *Langmuir* **18** 1466
[29] Michot L J, Ghanbaja J, Tirtaatmadja V and Scales P J 2001 *Langmuir* **17** 2100
[30] Rowan D and Hansen J-P 2002 *Langmuir* **18** 2063
[31] Belloni L 2000 *J. Phys.: Condens. Matter* **12** R549
[32] Rowan D, Hansen J-P and Trizac E 2000 *Mol. Phys.* **98** 1369
[33] Alexander S, Chaikin P M, Grant P, Morales G J and Pincus P 1984 *J. Chem. Phys.* **80** 5776
[34] Belloni L 1998 *Colloids Surf. A: Physicochem. Eng. Aspects* **140** 227
[35] Hansen J-P and Löwen H 2000 *Ann. Rev. Phys. Chem.* **51** 209
[36] Hsu J-P and Tseng M T 1997 *Langmuir* **13** 1810
[37] Trizac E 2000 *Phys. Rev.* E **62** R1465
[38] Trizac E, Bocquet L and Aubouy M 2002 *Preprint* cond-mat/0201510 submitted
[39] Groot R D 1991 *J. Chem. Phys.* **95** 9191
[40] Monovoukas Y and Gast A P 1989 *J. Colloid Interface Sci.* **128** 533
[41] Robbins M O, Kremer K and Grest G S 1988 *J. Chem. Phys.* **88** 3286
[42] Meijer E J and Frenkel D 1991 *J. Chem. Phys.* **94** 2269
[43] Bitzer F, Palberg T, Löwen H, Simon R and Leiderer P 1994 *Phys. Rev.* E **50** 2821
[44] Eppenga R and Frenkel D 1984 *Mol. Phys.* **52** 1303
[45] Veerman J A C and Frenkel D 1992 *Phys. Rev.* A **45** 5632
[46] Hansen J-P 1981 *J. Phys. C: Solid State Phys.* **14** L151